A cortactin *CTTN* coding SNP contributes to lung vascular permeability and inflammatory disease severity in African descent subjects

PATRICK BELVITCH, NANCY CASANOVA, XIAOGUANG SUN, SARA M. CAMP, SAAD SAMMANI, MARY E. BROWN, JOSEPH MASCARHENAS, HEATHER LYNN, DJANYBEK ADYSHEV, JESSICA SIEGLER, ANKIT DESAI, LALEH SEYED-SAADAT, ALICIA RIZZO, CHRISTIAN BIME, GAJENDRA S. SHEKHAWAT, VINAYAK P. DRAVID, JOHN P. REILLY, TIFFANIE K. JONES, RUI FENG, ELEFTHERIA LETSIOU, NUALA J. MEYER, NATHAN ELLIS, JOE G.N. GARCIA*, and STEVEN M. DUDEK*

CHICAGO, AND EVANSTON, ILLINOIS; TUCSON, ARIZONA; MINNEAPOLIS, MINNESOTA; INDIANAPOLIS, INDIANA; AND PHILADELPHIA, PENNSYLVANIA

The cortactin gene (CTTN), encoding an actin-binding protein critically involved in cytoskeletal dynamics and endothelial cell (EC) barrier integrity, contains single nucleotide polymorphisms (SNPs) associated with severe asthma in Black patients. As loss of lung EC integrity is a major driver of mortality in the Acute Respiratory Distress Syndrome (ARDS), sepsis, and the acute chest syndrome (ACS), we speculated CTTN SNPs that alter EC barrier function will associate with clinical outcomes from these types of conditions in Black patients. In case-control studies, evaluation of a nonsynonymous CTTN coding SNP Ser484Asn (rs56162978, G/A) in a severe sepsis cohort (725 Black subjects) revealed significant association with increased risk of sepsis mortality. In a separate cohort of sickle cell disease (SCD) subjects with and without ACS (177 SCD Black subjects), significantly increased risk of ACS and increased ACS severity (need for mechanical ventilation) was observed in carriers of the A allele. Human lung EC expressing the cortactin S484N transgene exhibited: (i) delayed EC barrier recovery following thrombin-induced permeability; (ii) reduced levels of critical Tyr486 cortactin phosphorylation; (iii) inhibited binding to the cytoskeletal regulator, nmMLCK; and (iv) attenuated EC barrier-promoting lamellipodia dynamics and biophysical responses. ARDS-challenged Cttn+/− heterozygous mice exhibited increased lung vascular permeability (compared to wild-type mice) which was significantly attenuated by IV delivery of liposomes encargoed with CTTN WT transgene but not by CTTN S484N transgene. In summary, these studies suggest that the CTTN S484N coding SNP contributes to severity of

*Denotes co-senior authors.

From the Division of Pulmonary, Critical Care, Sleep and Allergy, Department of Medicine, University of Illinois at Chicago, Chicago, Illinois; De-Department of Medicine, University of Arizona Health Sciences, Tucson, Arizona; University of Minnesota, Minneapolis, Minnesota; Department of Medicine, Indiana University, Indianapolis, Indiana; Department of Materials Science and Engineering, Northwestern University, Evanston, Illinois; Division of Pulmonary, Allergy, and Critical Care Medicine and Lung Biology Institute, University of Pennsylvania Perelman School of Medicine, Philadelphia, Pennsylvania; Department of Biostatistics, Epidemiology, and Informatics, University of Pennsylvania Perelman School of Medicine, Philadelphia, Pennsylvania.

Submitted for Publication August 17, 2021; revision submitted January 20, 2022; Accepted for Publication February 10, 2022.

Reprint requests: Steven M. Dudek, Division of Pulmonary, Critical Care, Sleep, and Allergy, Department of Medicine, University of Illinois at Chicago, CSB 915, 840 S. Wood St., Chicago, IL 60612 e-mail: sdudek@uic.edu.

1931-5244/$ - see front matter

https://doi.org/10.1016/j.trsl.2022.02.002

inflammatory injury in Black patients, potentially via delayed vascular barrier restoration. (Translational Research 2022; 000:1–19)

Abbreviations: ACE = Angiotensin-converting enzyme; ACS = Acute chest syndrome; AFM = Atomic force microscopy; ARDS = Acute respiratory distress syndrome; BAL = Bronchoalveolar lavage; CTTN = Cortactin gene; DOPE = dioleoylphosphatidylethanolamine; DOTAP = *N*-((dioleoyloxy)propyl)-*N,N,N,*-trimethylammonium chloride; EC = Endothelial cell; ECIS = Electric Cell-substrate Impedance Sensing; EGF = Epidermal growth factor; EGFP = Enhanced green fluorescent protein; HGF = Hepatocyte growth factor; HLMVEC = Human lung microvascular endothelial cells; HPAEC = Human pulmonary artery endothelial cells; IF = Immunofluorescence; IP = Immunoprecipitation; IV = Intravenous; KO = Knockout; LPS = Lipopolysaccharide; MLC = Myosin light chain; MV = Mechanical ventilation; *MYLK* = Non-muscle myosin light chain kinase gene; NAMPT = Nicotinamide phosphoribosyltransferase; nmMLCK = Non-muscle myosin light chain kinase protein; NTA = N-terminal acidic region; PEEP = Positive end-expiratory pressure; S1P = Sphingosine-1-phosphate; SB = Spontaneously breathing; SCD = Sickle cell disease; SNP = Single nucleotide polymorphism; TER = Trans-endothelial electrical resistance; VILI = Ventilator induced lung Injury; WT = Wild-type

Brief Commentary
Belvitch, et al.

Background

The acute respiratory distress syndrome (ARDS) is a severe inflammatory lung injury characterized by a loss of endothelial barrier function and vascular leak with increased susceptibility and mortality observed in patients of African descent. Cortactin is an actin binding-protein critical to cellular responses that determine barrier function and contains multiple single nucleotide polymorphisms (SNPs) which may account for disparities in severe inflammatory lung injury.

Translational Significance

We identify a cortactin gene coding SNP (rs56162978) associated with inflammatory lung injury risk and severity in African descent subjects. Lung endothelial cells and animals expressing this SNP transgene demonstrate impaired barrier function and increased pulmonary vascular leak.

INTRODUCTION

Acute Respiratory Distress Syndrome (ARDS), the most severe form of inflammatory acute lung injury (ALI), is a devastating clinical condition associated with high mortality for which there is no effective pharmacologic treatment.[1,2] Sepsis or pneumonia caused by various pathogens, such as SARS-CoV-2, influenza, and multiple types of bacteria, are common causes of ARDS and lung inflammation.[3-6] The ongoing COVID-19 pandemic has highlighted the racial and ethnic differences in susceptibility and mortality due to ARDS,[7-10] with patients of African descent at higher risk.[11] In addition to health disparities due to bias and insufficient resource allocation, this observation also suggests that identification of genetic biomarkers that associate with ARDS risk and outcome may further improve risk stratification and therapeutic targeting.[9,12] We previously have identified and characterized several genetic ARDS biomarkers and potential therapeutic targets, such as nicotinamide phosphoribosyltransferase (*NAMPT*),[13,14] *MYLK* (encoding nonmuscle myosin light chain kinase or nmMLCK),[15-17] the growth arrest and DNA damage-inducible gene (*GADD45a*),[18] the sphingosine-1-phosphate (S1P) receptor 3,[19] and *SELPLG* (encoding P-selectin glycoprotein ligand 1).[20]

A common mechanistic theme of the proteins encoded by genes harboring ARDS-associated single nucleotide polymorphisms (SNPs) is their participation in modulating pulmonary vascular permeability in response to inflammatory stimuli, a key pathologic feature of ARDS.[2,21-23] ARDS pathogenesis involves inflammation-induced disruption of the alveolar-vascular barrier, loss of endothelial cell (EC) barrier integrity and subsequent leakage of protein-rich fluid and inflammatory cells into the airspaces of the lungs leading to severe hypoxemia.[2,21-24] COVID-19 infection, in particular, induces a distinct vascular endotype of ARDS characterized by profound lung EC permeability, thrombosis and microangiopathy.[25-27] Formation of paracellular gaps between EC is determined by the structure and arrangement of the actin cytoskeleton and is critical to loss of vascular barrier integrity.[22,28]

We have previously defined an important role for the actin-binding protein, cortactin, in regulating cytoskeletal dynamics that determine EC barrier integrity[28-33] via localization at the EC periphery within lamellipodia where it contributes to spatially specific dynamic actin

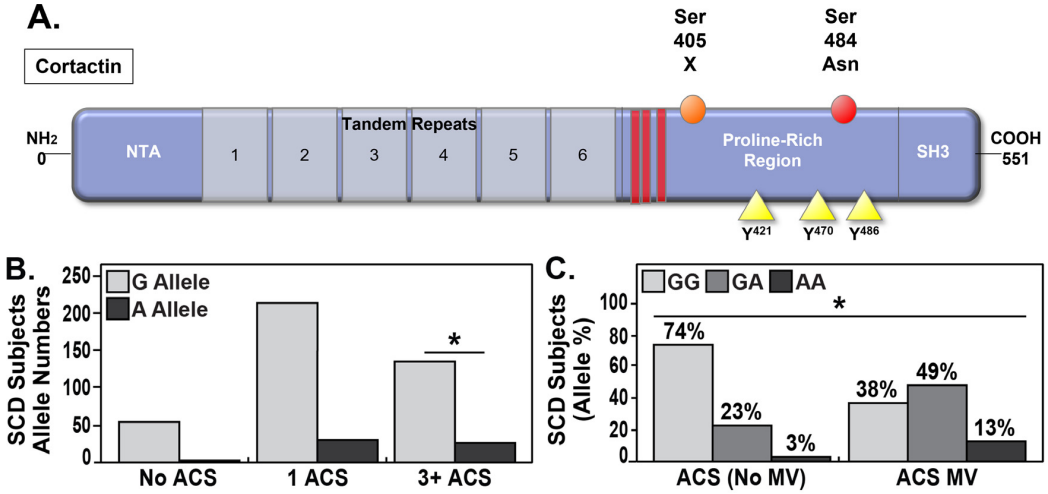

Fig 1. Cortactin coding SNP S484N is associated with the development and severity of acute chest syndrome (ACS) in subjects with sickle cell disease (SCD). **A)** Schematic diagram of cortactin protein is shown highlighting an N-terminal acidic region which interacts with Arp 2/3 complex to stimulate actin polymerization, a series of actin-binding tandem repeats and a Src homology 3 (SH3) domain which interacts with multiple regulatory proteins. A key proline-rich region near the C-terminus (AA #401-495) contains serine and tyrosine phosphorylation sites (including Y^{486}) that regulate cortactin function. Also shown are the location of the *CTTN* coding SNP representing a serine to asparagine substitution at AA #484 (S484N). **B)** Genotyping of rs56162978 in 177 SCD subjects with 0 episodes of ACS, 1 episode, or more than 3 episodes identified the overwhelming predominance of the G allele in SCD subjects without a prior ACS episode (55 G alleles, 3 A alleles). In contrast, the prevalence of the rs56162978 A allele was significantly increased in SCD individuals with one or more ACS episodes (OR 3.43), with significant increased A alleles in SCD subjects experiencing multiple ACS episodes (OR 3.75)**. C)** Depicted is the association between *CTTN* SNP rs56162978 genotypes and acute chest syndrome severity as defined by ACS requiring mechanical ventilation. A strong association exists between the rs56162978 A allele and SCD/ACS severity. Fewer SCD subjects with the GG genotype required mechanical ventilation compared with either the GA or AA genotype. consistent with the *CTTN* Ser 484Asn coding SNP conferring increased ACS severity**.** The asterisk refers to T-test comparisons between identical prevalence of *CTTN* rs56162978 genotypes in the two groups (ACS no MV and ACS with MV, $P < 0.05$).

rearrangement and branched actin polymerization.[34-37] Cortactin's multidomain structure (Fig 1A) integrates the effects of several signaling and structural elements, including an N-terminal acidic region which stimulates actin polymerization via the Arp 2/3 complex, and tandem repeats that facilitate actin binding. The cortactin C-terminal SH3 domain allows for interaction with other cytoskeletal regulatory proteins[35] including an interaction with nmMLCK which mediates barrier enhancement by S1P.[29,33] Cortactin exhibits a proline-rich region containing multiple serine and tyrosine phosphorylation sites which are targets for several kinases associated with cytoskeletal rearrangement including Src, c-Abl/Arg, Fer, and Fyn.[33,37-39] Phosphorylation of 3 critical residues, Tyr^{421}, Tyr^{466}, and Tyr^{482}/Tyr^{486} in mouse/human cortactin respectively, regulates cortactin cytoskeletal activity in EC.[37,40] We have previously shown that decreased cortactin expression significantly attenuates pulmonary EC barrier enhancement by barrier-enhancing stimuli such as S1P, ATP, and HGF.[29,41-43] Furthermore, cortactin-deficient mice demonstrate increased intradermal vascular permeability following histamine injection.[44,45]

Despite this background strongly implicating cortactin in processes relevant to ARDS pathophysiology, the potential of *CTTN* as an ARDS candidate gene is unknown. Several SNPs within the *MYLK* gene (encoding nmMLCK) are associated with increased ARDS risk in subjects of African descent[15-17] and directly contribute to loss of EC barrier recovery.[46] We previously reported that *CTTN* contains a common intronic SNP that is associated with differential susceptibility to severe asthma which, like ARDS, is a serious inflammatory lung disorder.[47]

The current study was designed to assess *CTTN* as a candidate gene in inflammatory lung injury and to functionally characterize *CTTN* variants that potentially contribute to altered EC barrier responses. We identified a nonsynonymous *CTTN* exonic SNP (rs56162978) as significantly associated with clinically relevant outcomes in

Black subjects: mortality in patients with sepsis, and risk of acute chest syndrome (a form of inflammatory lung injury) in sickle cell disease subjects (SCD-ACS). Structure/function analysis showed the S484N SNP to be in close proximity to the critical Tyr^{486} site strongly involved in EC motility[40] and cytoskeletal rearrangement.[38] In a limited prior study, we demonstrated that lung EC expressing this *CTTN* variant exhibit impaired wound closure, cell locomotion, and reduced responses to the EC barrier-protective agonist, S1P.[31] The present study confirms *CTTN* as a candidate gene in Black patients with sepsis or inflammatory lung injury and interrogates the functionality of the S484N SNP in EC barrier responses. *In vitro* studies demonstrate that the S484N SNP alters levels of Tyr^{486} phosphorylation and cortactin binding to nmMLCK, as well as reduces EC barrier-promoting lamellipodia dynamics. *In vivo* studies utilizing ventilator-induced lung injury (VILI)-exposed $Cttn^{+/-}$ heterozygous mice demonstrate that delivery of the *CTTN* S484N transgene fails to improve lung injury, whereas delivery of the *CTTN* WT transgene significantly attenuates VILI-induced vascular leak. Together, these results strongly support a critical role of cortactin in vascular barrier restoration during inflammatory lung edema and injury and highlight the potential contribution of the CTTN S484N coding SNP to the severe ARDS and other inflammatory health disparities observed in Black patients.

MATERIAL AND METHODS

***CTTN* coding SNP selection and genotyping of *CTTN* SNP rs56162978 G/A in Black controls and sickle cell disease subjects.** We previously reported the initial search for common variations in the *CTTN* gene[47] by sequencing of exon and flanking regions utilizing DNA from ARDS and healthy controls (19 Black, 29 Non-Hispanic Whites). This revealed a single *CTTN* coding SNP, rs56162978, resulting from G/A variation and encodes the S484N protein polymorphism. We investigated the association between rs56162978 G/A and respiratory phenotypes by genotyping a series of Blacks with sickle cell disease (SCD) utilizing DNA and clinical phenotypic information from a previously reported cohort of adult sickle cell disease subjects recruited from outpatient clinics at the University of Chicago (UCH) and at the University of Illinois at Chicago (UIC).[48-50] Genotyping for the rs56162978 *CTTN* SNP was performed in 177 adult sickle cell patients and 187 controls of African descent. Demographic and sickle cell phenotype information are summarized in Table 2. Associations were analyzed using SNPstats.

Genotyping of *CTTN* SNP rs56162978 G/A in Black controls and sepsis subjects. We analyzed DNA and clinical phenotyping information from an extension of a previously reported cohort of sepsis subjects,[51,52] which now includes 725 that genomically clustered with the 1000 Genomes ASW population described as "people with African ancestry in Southwest United States." As a nonsynonymous coding SNP, we used additive, dominant, and recessive models to test the association of the rs56162978 *CTTN* SNP with sepsis mortality after adjusting for genetic ancestry with the first 2 components derived from multidimensional scaling using all genotyped variants. Logistic regression (chi squared test) was used to test for association between sepsis nonsurvival and genotype using 3 separate models: Additive (coding genotype as 0-1-2 copies); dominant (coding 0-1); and recessive (coding 0-1). Demographic and phenotypic information are briefly summarized for this cohort in Table 1.

Reagents. Unless otherwise specified, reagents and antibodies were obtained from Millipore-Sigma (St. Louis, MO). The cationic phospholipid *N*-[(dioleoyloxy)propyl]-*N,N,N*,-trimethylammonium chloride (DOTAP) and the neutral phospholipid dioleoylphosphatidylethanolamine (DOPE) were purchased from Avanti Polar Lipids (Alabaster, AL). Mouse monoclonal α-cortactin-phospho-Y-486 (# AB3853) antibody was obtained from Merck Millipore (Darmstadt/Germany). Mouse angiotensin-converting enzyme (ACE) antibody was obtained from R&D Systems (Minneapolis, MN). Reagents for western blotting were purchased

Table 1. Clinical demographic and phenotypic data of the sepsis cohort

rs56162978 A/G	GG (n = 504)	GA (n = 204)	AA (n = 17)
Age in years, mean SD	60.1 ± 16.0	60.2 ± 16.8	61.2 ± 12.8
APACHE III score, median IQR	84 (60–118)	87 (63–123)	114 (99–144)
AKI, N (%)	271/439 (62%)	114/185 (62%)	12/15 (80%)
Excludes 86 subjects with pre-existing ESRD or AKI			
30-day mortality	161 (31.9%)	59 (28.9%)	10 (58%)

Abbreviations: APACHE, Acute Physiologic Assessment and Chronic Health Evaluation; AKI, acute kidney injury; ESRD, end stage renal disease.

from Bio-Rad (Hercules, CA). Immobilon-P transfer membrane was purchased from Millipore Corp. (Bedford, MA).

Cell culture. Human lung microvascular endothelial cells (HLMVEC) and human pulmonary artery EC (HPAEC) were obtained from Lonza (Walkersville, MD) and cultured as described previously.[53] Cells were used at passages 5−7 for all experiments.

Transfections. The following plasmids produced in our laboratory were used for experiments: c-myc-tagged cortactin wild-type (S484; WT), c-myc-tagged cortactin S484N SNP (S/N), c-myc-tagged cortactin S484N and Y486F (S/N-Y/F; double mutation), EGFP-tagged cortactin WT, EGFP-tagged cortactin S484N,[31] or c-myc-Flag-tagged MLCK. Lung endothelial cells were transfected with the plasmids using X-fect transfection reagents (Takara Bio) per manufacturer protocol.

Measurement of trans-endothelial electrical resistance (TER). ECIS (Electric Cell-substrate Impedance Sensing) was used to assess the EC barrier function, as we have described previously in detail.[53] In this assay, EC were grown to confluence on 8W10E+polycarbonate arrays (Applied Biophysics, Troy, NY) and treated as indicated. TER measurements were recorded and plotted vs time using the Epool software.

Generation of CRISPR EC expressing *CTTN* Ser484Asn SNP. Homozygous amino acid substitution *CTTN* S484N was created using CRISPR/Cas9 technologies in the University of Arizona Cancer Center Genome Editing Facility. Cas9 protein and guide RNAs (crRNAs and tracrRNA) were obtained from Integrated DNA Technologies. The guide RNA for cutting was 5′-ATCGTTCTCGTACTCATCGT-3′ and single-stranded donor DNA was 5′-TTGTATTGTTCAGCTCTGTCATGGCTTTCTTTTA GAGGACAGCACCTAC GATGAGTACGAGAACGATCTGGGGATCACAGCCGTCGCCCTGTACGACTAC-3′. Parental hTERT-transformed human aorta endothelial cells (teloHAECs) were transfected using the Lipofectamine RNAiMAX reagent (Thermo Fisher Scientific). Two days after transfection, cutting efficiency was estimated based on DNA prepared from a portion of the transfected cell population using a T7 endonuclease assay (New England BioLabs) using PCR primers flanking the site of the nucleotide substitution (5′-TAGGCACATTTGGGGCATCG-3′ and 5′-CGAACATCAAGGCAT CTGTGC-3′). Single cells were deposited in ten 96-well plates by Human Immune Monitoring and Flow Cytometry service. Colonies were expanded and DNA prepared and screened by PCR and direct sequencing (Eurofins Genomics). Generation of the homozygous clone required 2 rounds of editing; the first to generate a heterozygous line and then a second to generate homozygous clones. RT-PCR analysis confirmed the presence of the homozygous nucleotide substitution and Western blot analysis confirmed the presence of the CTTN protein. These cells were expanded and plated in 96 well TER dishes (Applied Biophysics). Cells were treated with LPS (10 μg/ml), and TER was assessed. TER measurements were plotted using the Applied Biophysics software.

Immunoprecipitation (IP). IP was performed as described before in detail.[54] Briefly, cell lysates were immunoprecipitated with an anti-cmyc or anti-Flag antibodies overnight at 4˚C, followed by addition of protein G beads (GE Life Sciences, Pittsburg, PA). Proteins were eluted for the beads and processed for immunoblotting.

Immunoblotting. Equal amounts of protein samples were mixed with Laemmli sample buffer, boiled, and subjected to SDS-PAGE electrophoresis. After transfer to PVDF membrane, blots were incubated with primary antibodies overnight, following an hour incubation at room temperature with horseradish peroxidase-conjugated secondary antibodies (Cell Signaling Technology, Danvers, MA). The bands were visualized using the Pierce ECL Western Blotting substrate (ThermoScientific, Rockford, IL). Band densities were determined using the Image J software (National Institutes of Health).

Immunofluorescence. EC transfected with EGFP-cortactin constructs (WT and S484N) were stimulated at 37˚C with S1P (1 μM) for 2 and 30 minutes. Cells were fixed and then stained with and a phospho-Tyr 486 cortactin antibody and phalloidin-AlexaFluor 633 (for actin staining), using previously published immunofluorescence protocols.[46] Images were taken on a Leica TCS SP5 AOTF laser-scanning confocal microscopy system scanning at 400 Hz. Twelve-bit 512 × 512 images were acquired sequentially (with a line average setting of 16) with Leica LAS AF software and detected with a photomultiplier tube. All postacquisition image processing was performed with the ImageJ software bundle (http://rsb.info.nih.gov/ij/).

Kymography. Live cell imaging and kymographic analysis were completed as previously described.[54] Briefly, EC were plated onto gelatin-coated coverslips, placed in a recording chamber (ALA Scientific Instruments, Westbury, NY) and overlayed with media containing 2%FBS. Experiments were performed with the recording chamber placed on a heated stage to maintain a temperature of 37˚C. A Zeiss 710 laser scanning confocal microscope was used for to acquire Images every 6 seconds. Cells were observed under basal conditions, and for at least 20−30 minutes following administration of 1 μM S1P to capture membrane protrusions. Time series images were processed using ImageJ. The Multiple Kymograph plugin was used to quantify

membrane protrusion dynamics as described previously.[55-57] N = 6 individual cells with 10−15 protrusion events were analyzed for each condition.

Atomic force microscopy. AFM imaging and force measurements were performed on live HPAEC as previously described.[58-60] utilizing a 37°C heating stage and a BioScope Catalyst atomic force microscope with a Nanoscope V controller (Bruker, Inc.) residing atop of a Axio Oberver.D1m inverted optical microscope (Carl Zeiss, Inc. Oberkochen, Germany). A ScanAsyst-Fluid probe (Bruker) was used with a nominal spring constant $k \sim 0.7$ Nm^{-1} and a nominal tip radius $R \sim 20$ nm. EC transfected with EGFP-tagged cortactin WT, EGFP-tagged cortactin S484N, or EGFP-vector[31] were identified via optical microscopy, and then an appropriate cell periphery area was selected to enable subcellular determination of cellular biomechanical properties. Measurements included analysis of 64 × 64 loading-unloading curves (force-volume map), with force-volume maps acquired over ∼18 minutes at each time point. Elastic moduli were then calculated as previously described.[58-60]

Cortactin-nmMLCK binding assay. GST-tagged cortactin fusion proteins and recombinant nmMLCK were produced in our laboratories as previously described.[32] Recombinant protein binding assays were then performed as modified from prior protocol.[32,33] First, cortactin constructs were incubated with recombinant $p60^{src}$ kinase or buffer alone to generate phosphorylated or control proteins prior to nmMLCK incubation. Src phosphorylation was performed as follows: purified GST-labeled cortactin proteins were dialyzed and brought to 0.1 mg/ml concentration using reaction buffer containing 25 mM Tris−HCl, pH 7.5, 20 mM KCl, 5 mM Mg-acetate, and 0.5 mM leupeptin. Phosphorylation of proteins in reaction buffer was initiated with 0.2 mM ATP and 75 U/ml recombinant $p60^{src}$ kinase. Kinase reactions were performed at 22°C for 5 minutes. GST-tagged cortactin was then loaded onto glutathione−Sepharose beads (Amersham) at concentrations of 10 μg per 100 μl reaction. Flag-MLCK proteins were added at concentrations of 0.1 μM in buffer (20 mM Tris, pH 7.5, 100 mM KCl, 1 mM $MgCl_2$, 0.2 mM DTT, 1% Triton X-100, and 1% BSA) and incubated at room temperature for 20−30 minutes. The beads were then pelleted, washed with PBS to remove unbound protein, and protein binding analyzed by SDS−PAGE and Western blotting.

Murine models of LPS- and ventilator-induced lung injury (VILI). All experiments and animal care procedures were approved by the University of Illinois at Chicago Animal Care and Use Committee. Experiments were performed on 8−12 week-old male *CTTN*$^{+/-}$ mice generated on a C57BL/6J background (Jackson Laboratory, Bar Harbor, ME).[61] Animals were anesthetized with ketamine/xylazine (100/5 mg/kg) and injected intratracheally with LPS (1 mg/kg) or PBS (control mice). The respiratory failure and hypoxemia caused by ARDS often requires supportive treatment with invasive mechanical ventilation (MV),[62] however, positive pressure ventilation also contributes to lung injury, a process termed ventilator-induced lung injury (VILI).[63] For the VILI model, anesthetized mice were connected to a small-animal ventilator (Harvard Apparatus, Boston, MA) in room air, with a tidal volume of 30 ml/kg, 75 breaths per minute, and a positive expiratory pressure (PEEP) of 0 cm H_2O. Normal saline (0.2 ml) was given via intraperitoneal injection at the onset of ventilator use and after 2 hours to all ventilated mice. Spontaneously breathing mice (SB) were used as controls. At the end of the experiment (18 hours after LPS and 4 hours after VILI), bronchoalveolar lavage (BAL) fluid and lungs were harvested immediately. BAL was collected by instilling 1 ml Hanks' balanced salt solution through the tracheal cannula into the lungs. The recovered fluid was centrifuged to separate the BAL cells from the BAL fluid, and total protein and cell counts were measured as described previously.[64] Differential counting was performed in BAL total cells using the Kwik-Diff stain kit (ThermoFisher). Lung tissues were embedded in paraformaldehyde for histologic analysis.

ACE antibody-conjugated liposome delivery of cortactin plasmids. Liposomes were generated as previously described with minor modifications.[65] Briefly, the liposomes were generated using a 1:1 molar ratio of DOTAP/DOPE, dissolved in chloroform to a concentration of 10 mg/ml. The solvent was evaporated in a water bath set at 50^0C under nitrogen gas. The resulting dry lipid film was immediately re-suspended in 100 μl of PBS (pH 7.4; final concentration, 20 mg/ml). The cationic lipid dispersion was combined with plasmid DNA (pc3.1, WT *CTTN*, or S484N SNP *CTTN*) (1 μg per 10 μg lipid) in a glass container. The liposome/DNA mixture was sonicated to clarity in a water bath sonicator. For the ACE antibody, primary amines were blocked with sulfo-N-hydroxysuccinimide (NHS) acetate in PBS (pH 7.4), and incubated for 1 hour at room temperature. The solution was then filtered with a 30-kDA Ultrafree-MC filter (Millipore, Danvers, MA) and adjusted to a final concentration of 0.2 mg/ml. The modified ACE antibody was crosslinked to liposomes containing the *CTTN* DNA by covalently linking the carboxyl groups on the ACE antibody with the amine groups on liposomes, using 1-ethyl-3-[3-dimethylaminopropyl] carbodiimide hydrochloride (EDC) reagent (Pierce, Rockford, IL) as described in the

manufacturer's protocol. Labeled liposomes were purified by dialysis in 20 kDa Slide-A-Lyzer (Thermo Scientific) against a 1,000-fold excess volume of sterile PBS (pH 7.4) overnight. A 100 μl aliquot of sterile ACE-conjugated liposomes (containing 10 mg/kg DNA) was injected intravenously into the internal jugular vein 24 hours before VILI experiments.

Immunohistochemistry. To determine the expression of ACE-liposome targeted cortactin plasmids in mouse lung tissue, paraffin blocks of lung tissues were prepared and 10 μm microscope slides obtained. Serial sections of each specimen were deparaffinized and rehydrated in serial graded ethanol. Antigens were retrieved with 50 mM citrate buffer, pH 6.4 and by heating slides in a 98˚C water bath, for 15 minutes. Endogenous peroxidase activity was blocked in methanol containing 3% hydrogen peroxide and endogenous biotin was blocked with avidin biotin block. After blocking with an IgG blocker and normal horse serum, the sections were incubated with a mouse monoclonal antibody to mouse c-myc (9E10, Sigma Chemical Company, St Louis, MO, USA) 1:500 dilution for 1 hour, followed by 30 minutes incubation with a biotin conjugated mouse secondary antibody (Vector Laboratories Inc., Burlingame, CA). The ABC complex and 3,3′-diaminobenzidine (Vector Laboratories, Inc., Burlingame, CA) solutions were used serially, and the slides were counterstained with hematoxylin.

Lung histology. Fixed lungs were embedded in paraffin and cut into 10 μm sections on slides. Slides were stained with hematoxylin and eosin (H&E) in research histology and tissue imaging core at the University of Illinois at Chicago. H&E-stained lung sections (n = 3−6 per condition) were scored by an investigator blinded to the experimental conditions. In each section, 5 fields were randomly scored for interstitial edema, neutrophil infiltration, and alveolar vacuolization at 20x magnification. Each parameter was scored from 0 to 4 (0 being none present, and 4 being severe and diffuse throughout the chosen field). Scores were added for each field and averaged to obtain a histologic lung injury score for each section. The composite lung injury score represents the mean injury scores for each condition on a scale of 0−12.

Statistical analysis. *In vitro* and *in vivo* data (Fig. 2−7): Results are expressed as mean ± SEM when comparing the differences between groups. Statistical analysis was performed using GraphPad Prism 8. Data were assessed for normality using Shapiro-Wilk normality test. The parametric methods of unpaired t-test or one-way ANOVA (Newman-Keuls *post hoc* test) were used to compare means between 2 or more groups respectively. Differences were considered to be statistically significant when $P < 0.05$. Clinical data analysis was performed using Golden Helix SNP and Variation Suite and PLINK v1.07 as we previously described.[20] As mentioned above in the patient cohort description, we used the chi square test for the association between SNP and outcome.

Table 2. Clinical demographic and phenotypic data of the sickle cell cohort

	Sickle cell patients	Controls
Median Age (range)	25 (18−73)	55 (24−93)
Mean Age	29.5	55.3
Female Sex (%)	53	93
Disease Phenotype (%):		
SS	75	N/A
SC	16.5	
S+Thalassemia	8.5	

RESULTS

Significant association of *CTTN* SNP rs56162978 with sepsis and sickle cell disease (SCD) severity in Blacks. We examined the associative frequency of rs56162978 with clinical outcomes in Black subjects with sepsis and sickle cell disease (SCD). Demographic and phenotypic information are briefly summarized for each cohort in Tables 1 and 2. The frequency of rs56162978 was 16% in the Penn sepsis African ancestry population, identical to that reported in the ASW African ancestry population in the Southwest United States and reported in 1000 Genomes project.[66] As seen in Table 3, carrying 2 copies of the rs56162978 SNP (AA, recessive model) was associated with increased risk of 30-day sepsis mortality

Table 3. *CTTN* rs56162978 SNP association with sepsis mortality

rs56162978A/G in African Ancestry sepsis cohort (n = 725);MAF 0.164	30 day nonsurvivors (AA/AG/GG)	30 day survivors (AA/AG/GG)	OR (95% CI)	*P* value
Additive model	10/61/171	7/143/333	1.06 (0.78- 1.44)	0.72
Dominant model	71/171	150/333	0.93 (0.66- 1.33)	0.72
Recessive model	10/232	7/476	3.07 (1.13- 8.38)	0.028

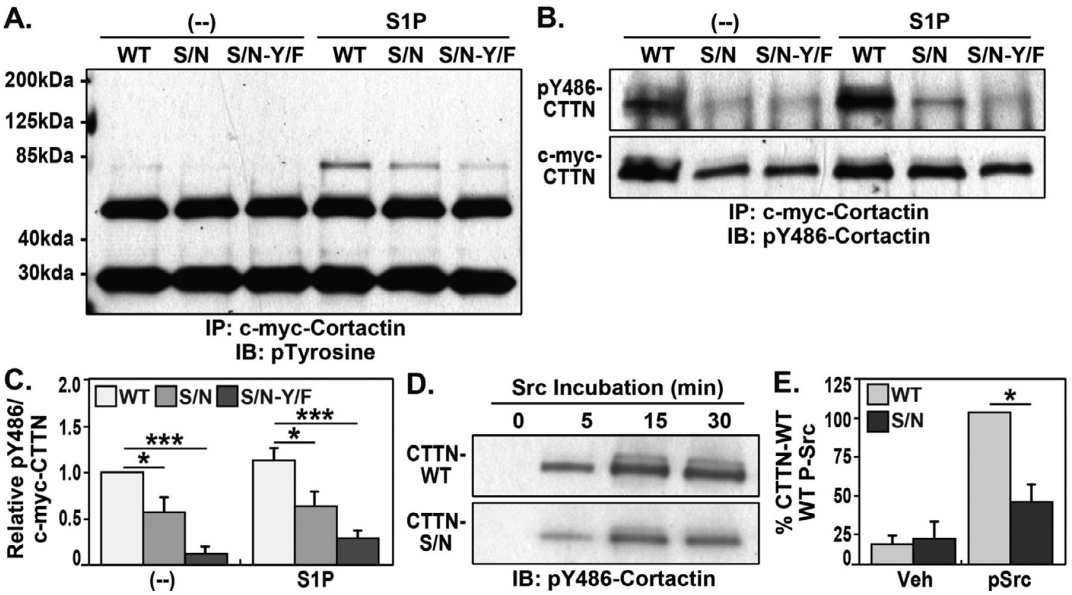

Fig 2. Cortactin SNP S484N decreases phosphorylation of a regulatory tyrosine residue. Human lung microvascular EC were transfected with c-myc-tagged cortactin constructs (WT, S/N, S/N Y/F) and then treated with S1P (1 μM, 2 min). Cortactin was immunoprecipitated from cell lysates with a c-myc antibody (~85 kDa). **A)** Shown is a representative western blot of immunoprecipitated c-myc-cortactin probed with an antibody against total phospho-tyrosine. (**B/C**) Shown is a representative western blot of immunoprecipitated c-myc-cortactin after vehicle or S1P (1 μM, 2 min) probed with antibodies directed against cortactin phospho-Y^{486} and c-myc. Quantified densitometry of these data (normalized to WT-vehicle condition) are shown from multiple independent experiments in **(C). (D/E)** Shown is a representative western blot of purified cortactin WT or S484N protein following incubation with Src kinase (0-30 min) and probed with antibodies directed against cortactin phospho-Y^{486}. Quantified densitometry of these data (normalized to WT-Src condition at 30 min) are shown from multiple independent experiments in **(E).** N = 3−5. * $P < 0.05$, *** $P < 0.001$.

in a cohort of 725 Black patients after adjusting for genetic ancestry (P= 0.028).

The association of the rs56162978 SNP with inflammatory lung disease in Blacks was further assessed by examining this association in adult Blacks with SCD (177 patients) with occurrences of the acute chest syndrome (ACS), a common form of ARDS in SCD subjects.[67,68] Genotyping of rs56162978 identified the overwhelming predominance of the G allele in SCD subjects without a prior ACS episode (55 G alleles, 3 A alleles; Fig 1B). In contrast, the prevalence of the rs56162978 A allele was significantly increased in SCD individuals with one or more ACS episodes (OR 3.43), with significant increased A alleles in SCD subjects experiencing multiple ACS episodes (OR 3.75; Fig 1B) Fig 1.C depicts a strong association of the rs56162978 A allele with SCD/ACS severity defined as requiring mechanical ventilation for the ACS episode. Fewer SCD subjects with the GG genotype required mechanical ventilation compared with either the GA or AA genotype, consistent with the *CTTN* Ser 484Asn coding SNP conferring increased ACS severity**.** Together, these data support the rs56162978 *CTTN* Ser 484Asn SNP as contributing to the risk and severity of inflammatory injury in Black subjects.

***CTTN* SNP S484N alters agonist-induced Tyr^{486} phosphorylation.** The rs56162978 *CTTN* S484N SNP results in an amino acid change from serine to asparagine at site 484 (S484N) that resides in close proximity to tyrosine 486 (Y^{486}) (Fig 1A), a functionally important site of Src/Abl-mediated phosphorylation.[29,37,38,40] To investigate whether Y^{486} phosphorylation is altered by the S484N SNP, lung EC were transfected with c-myc cortactin constructs harboring the wild type S484 (WT), the S484N SNP, and a double S484N-Y486F mutant in which the tyrosine at 486 has been eliminated as a tool to further assess the effects of S484N on phosphorylation at this specific site. C-myc cortactin was immunoprecipitated and pan-tyrosine phosphorylation measured (immunoblotting) under basal conditions and following stimulation with S1P (1 μM, 2 minutes), a well-established agonist for increasing Y^{486} phosphorylation.[29,33] Basal Tyr phosphorylation was very low, however, as expected, S1P increased total WT cortactin tyrosine phosphorylation, with reduced levels of cortactin tyrosine phosphorylation

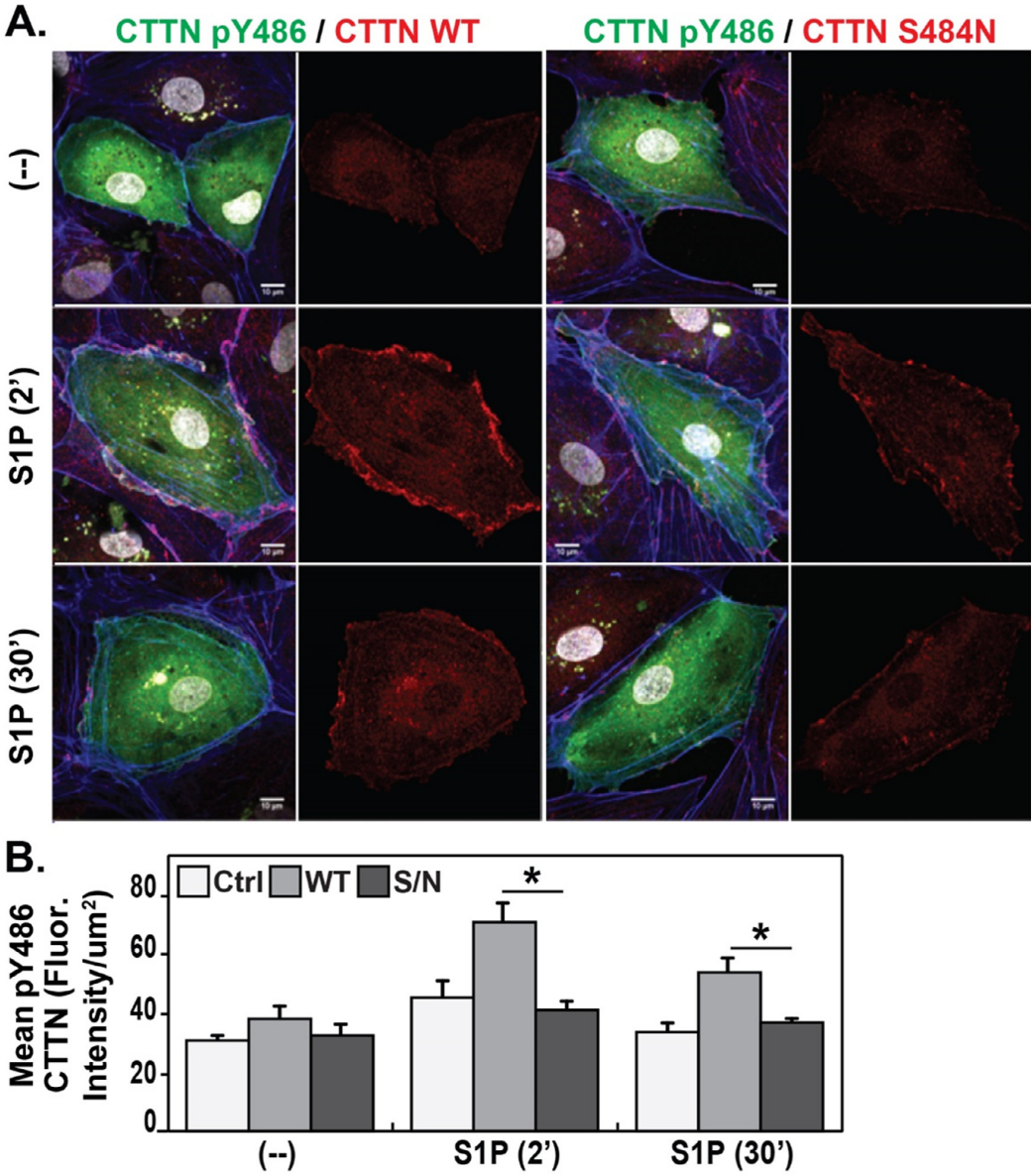

Fig 3. Cortactin SNP S484N reduces Y^{486} phosphorylation at the cell periphery. **A)** Representative immunofluorescence images of HLMVEC expressing EGFP-tagged WT or *CTTN* SNP S484N constructs (green) under basal conditions and following stimulation with S1P (1 μM, 2 and 30 min). Cells were fixed and stained for cortactin phospho-Y^{486} (red) and actin (purple) prior to imaging. **B)** Quantification of mean fluorescent intensity of cortactin phospho-Y^{486}. N = 3, * $P < 0.05$.

observed in the S484N and double-mutant S484N/Y486F constructs (Fig 2A). Complementary experiments designed to determine the specific site of cortactin phosphorylation employed a phospho-specific antibody directed against the Y^{486} site. Immunoblotting of immunoprecipitated c-myc cortactin with phospho-Y^{486} antibodies demonstrated significantly reduced Y^{486} phosphorylation in cortactin containing the S484N SNP or the double-mutant S484N/Y486F, compared to WT both at baseline and following S1P stimulation (Fig 2B). Relative Y^{486} phosphorylation per immunoprecipitated c-myc cortactin was quantified with each condition normalized to WT vehicle at baseline (S/N 0.572 $\pm$ 0.165; S/N-Y/F 0.136 $\pm$ 0.068) and

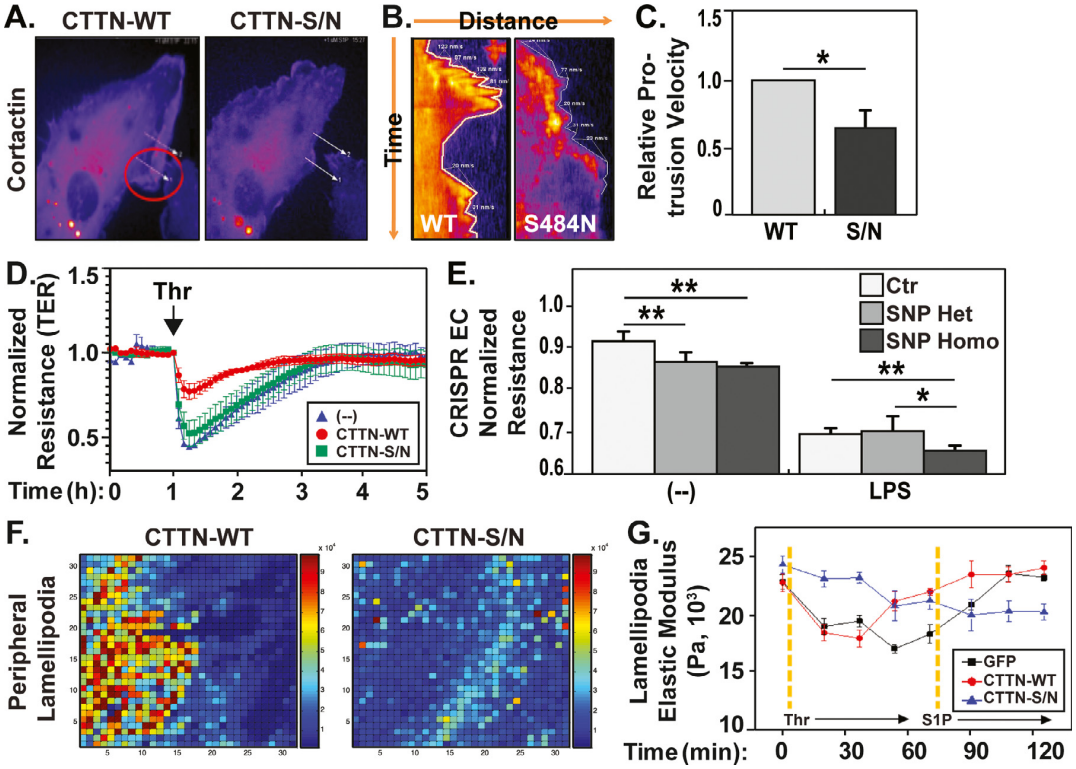

Fig 4. Cortactin S484N SNP alters endothelial protrusions and negatively affects barrier function. **A)** Representative live cell images of HLMVEC transfected with EGFP-WT or SNP S484N cortactin and stimulated with S1P (1 μM) to generate lamellipodia. **B)** Representative kymographs display cell membrane leading edge position over time to characterize membrane protrusion and retraction**. C)** Quantification of protrusion velocities in evolving lamellipodia normalized to WT cortactin. **D)** Trans-endothelial electrical resistance (TER) analysis of HPAEC transfected with control plasmid (Control), EGFP-tagged cortactin WT or S484N and treated with thrombin (1 U/ml). Pooled data was normalized to starting resistance. **E)** A human aortic EC line was genetically-edited by CRISPR to express either WT cortactin only, or one (heterozygote) or two (homozygote) S484N alleles and grown on the gold microelectrodes for TER measurements. Depicted is the significant reduction in basal normalized electrical resistance in S484N-containing EC compared to EC expressing WT cortactin. Moreover, TER measurements at 1 hr post LPS challenge (10 μg/mL) in EC homozygous for S484N exhibited significantly increased permeability compared to EC expressing either WT cortactin or one (heterozygote) S484N allele. **F)** Shown are representative histograms of elastic modulus levels in the peripheral regions of EC transfected with WT cortactin (left) or S484N cortactin (right). These histograms were obtained by AFM 30 min after S1P stimulation. Warmer colors (red) indicate higher values and cooler colors (blue) indicate lower values. **G)** HPAEC were transfected with EGFP-labeled WT cortactin (red lines), EGFP-S484N cortactin (blue lines), or EGFP plasmid control (black lines), and then peripheral cell regions were assessed by AFM to measure lamellipodia elastic modulus levels (in kPa) over time in response to thrombin (1 U/ml) and S1P (1 μM) sequentially as indicated (yellow dotted lines). N = 3–5. * $P < 0.05$, ** $P < 0.01$, *** $P < 0.001$.

following S1P (WT 1.144 ± 0.126; S/N 0.650 ± 0.140; S/N-Y/F 0.296 ± 0.080; Fig 2C). We next confirmed reduced Y^{486} phosphorylation in cortactin S484N-containing recombinant protein following incubation with Src kinase. At baseline, both WT-cortactin and S484N-cortactin proteins demonstrate low level Y^{486} phosphorylation which rapidly increases in WT-cortactin after Src kinase addition (5–30 minutes). In contrast, Y^{486} phosphorylation in the S484N-cortactin protein is attenuated (~50% of WT at 30 minutes) (Fig 2D, E).

CTTN SNP S484N-induced alterations in cortactin Y^{486} phosphorylation were further characterized by immunofluorescence microscopy of fixed lung EC after exposure to the barrier-enhancing agonist, S1P. EC transfected with EGFP control, WT or S484N EGFP-tagged constructs were probed for phospho-cortactin Y^{486} and co-stained for actin. S1P (1 μM, 2 minutes)

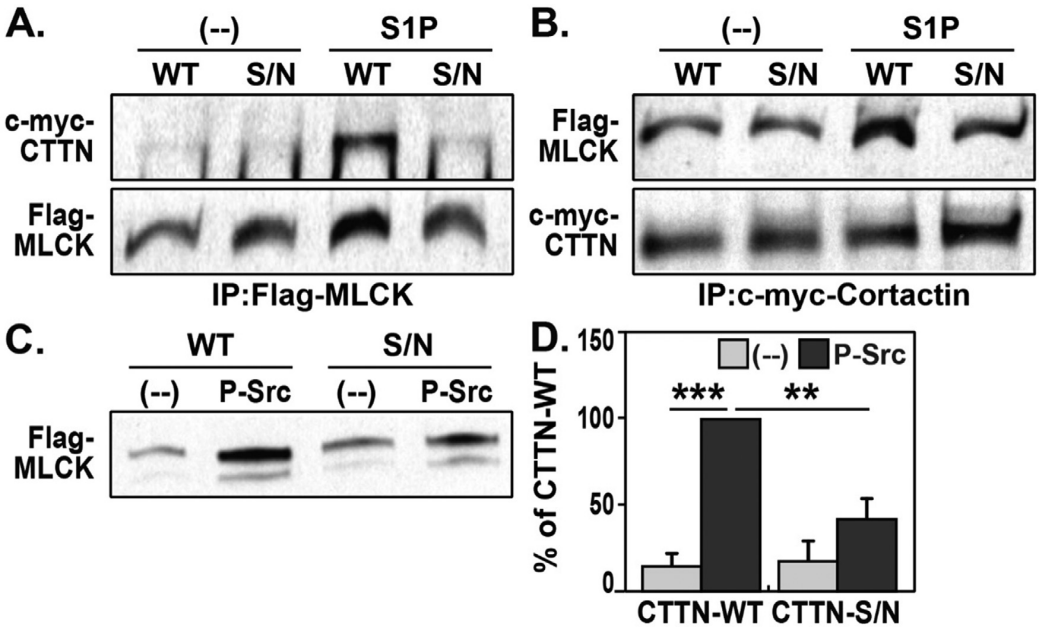

Fig 5. Cortactin S484N SNP reduces CTTN interaction with nmMLCK. **A-B)** HPAEC were co-transfected with FLAG-nmMLCK and c-myc-tagged cortactin (CTTN) WT or SNP S484N (S/N) constructs. Cells were then stimulated with vehicle (unstimulated) or S1P (1 μM, 10 min). nmMLCK or cortactin were immunoprecipitated and probed for associated proteins. Representative western blots show that S1P increases the cortactin-nmMLCK interaction in EC expressing the WT construct but not the S/N. **C)** Purified recombinant nmMLCK was incubated with WT or S/N cortactin proteins (GST-tagged) and Src kinase in reaction buffer for 5 min followed by immunoprecipitation of cortactin and blotted for nmMLCK. **D)** Densitometric quantification shows increased cortactin-nmMLCK binding following Src addition but this effect is attenuated by cortactin S/N. N = 3. ** $P < 0.01$, *** $P < 0.001$.

rapidly increased phosphorylated cortactin and F-actin at the periphery of EC transfected with the WT cortactin construct, but these effects were much less pronounced in EC transfected with S484N (Fig 3A). Fluorescent intensity of the phospho-cortactin Y^{486} signal was calculated for each condition and quantified in individual cells expressing the cortactin constructs. No significant differences were observed at baseline (no stimulation) between control, cortactin WT, and cortactin S484N (Fig 3B). However, following S1P (2 minutes), EC expressing cortactin S484N exhibit significantly decreased phospho-Y^{486} fluorescence compared to EC with WT cortactin, a pattern which persisted even after prolonged S1P stimulation (30 minutes).

***CTTN* SNP S484N alters EC membrane dynamics and barrier function.** Kymography uses live cell imaging to generate a timeline of cell protrusions that allows for quantitation of multiple parameters useful for analyses of lamellipodia dynamics, including protrusion velocity and distance, lamellipodia persistence, and retraction velocity.[69,70] To characterize the effects of S484N on EC lamellipodia function, lung microvascular EC were transfected with fluorescently tagged cortactin WT and S484N constructs and imaged via live cell microscopy over time to observe cell membrane protrusion and generate kymographs in order to characterize membrane dynamics (Fig 4A, B). Cells overexpressing cortactin S484N showed a significant 34% decrease in relative lamellipodia protrusion velocity compared to cells transfected with WT cortactin (Fig 4C), suggesting impaired ability to close intercellular gaps and increased permeability and consistent with our prior observations.[31]

The effect of cortactin S484N on EC barrier function was directly measured by trans-endothelial electrical resistance (TER) across pulmonary artery EC transfected with fluorescently tagged WT or S484N constructs. Cells expressing the constructs were selected by flow cytometry to enrich the percentage of transfected EC for subsequent EC permeability analysis and then grown on gold-plated electrodes. Baseline electrical resistance measurements were obtained followed by challenge with thrombin (1 U/ml) to disrupt barrier integrity. Cells over-expressing WT cortactin were significantly protected from thrombin-induced reductions

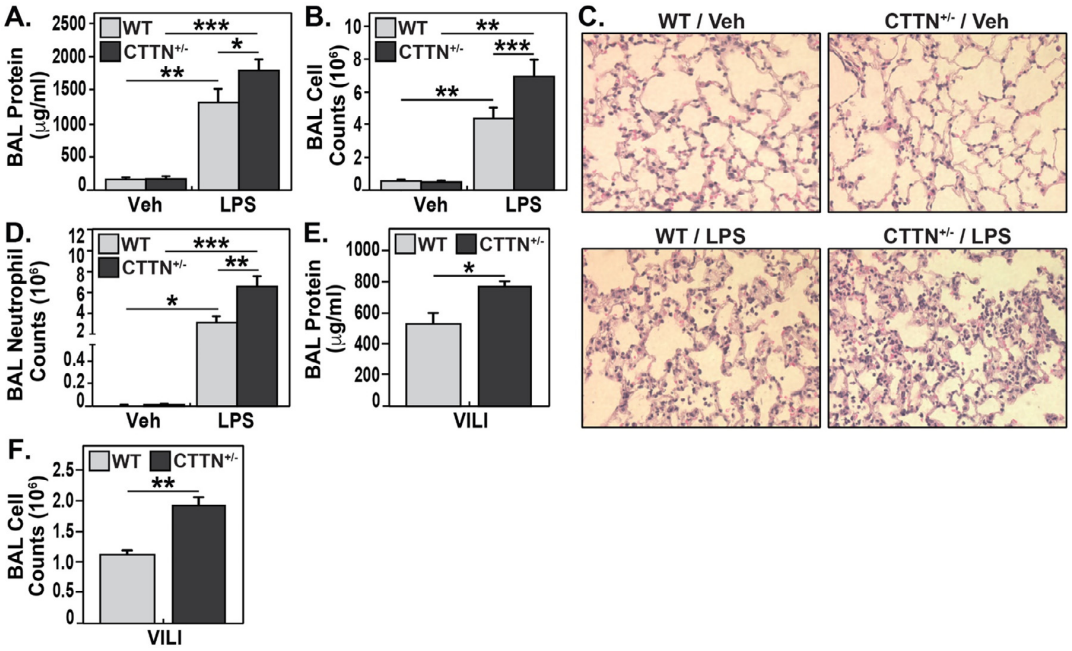

Fig 6. Cortactin deficiency exacerbates lung injury induced by LPS or mechanical ventilation. Cortactin heterozygous (*CTTN*+/-) and wild-type (WT) mice were treated with either **(A-D)** LPS (1 mg/kg, 18 hours) or **(E-F)** high-tidal volume mechanical ventilation (30 ml/kg, 4 hours; VILI model). Total protein content **(A)** and total cell counts **(B)** were determined in bronchoalveolar lavage (BAL) of mice treated with LPS or vehicle (PBS). **C)** Hematoxylin and eosin (H&E) staining of lung tissues obtained from control and LPS-treated *CTTN*+/- and WT mice. Shown are representative images (taken at 40x). **D)** Neutrophil accumulation into the alveolar space was assessed by differential count. Total protein content **(E)** and total cell counts **(F)** were determined in the BAL of $CTTN^{+/-}$ and WT mice after VILI. A-D, n = 3−8 mice per group; E-F, n = 4 mice per group. * $P < 0.05$, ** $P < 0.01$, *** $P < 0.001$.

in baseline TER compared to vector-transfected cells (Fig 4D). In contrast, EC over-expressing the cortactin S484N protein failed to exhibit this TER protection (Fig 4D). These results were confirmed in human aortic EC genetically edited by CRISPR to express either WT cortactin only, 1 (heterozygote) or 2 (homozygote) S484N alleles and grown on the gold microelectrodes for TER measurements Fig 4.E depicts the significant reduction in basal normalized electrical resistance in S484N-containing EC (0.865 ± 0.010 and 0.852 ± 0.004) compared to EC expressing WT cortactin (0.918 ± 0.009). Moreover, TER measurements at 1 hr post LPS challenge (10 μg/mL) in EC homozygous for S484N exhibited significantly reduced basal resistance (0.656 ± 0.004) compared to EC expressing either WT cortactin (0.695 ± 0.006) or one (heterozygote) S484N allele (0.703 ± 0.015). Taken together, these data indicate that expression of S484N cortactin has a detrimental effect on EC barrier function.

Changes in peripheral actin structure that are associated with increased EC barrier function[28,58,59] can be characterized by atomic force microscopy (AFM) with measurements of elastic modulus that are increased reflecting more robust actin polymerization and spatially directed tension development.[71] We previously utilized the subcellular resolution provided by AFM to demonstrate that c-Abl signaling and cortactin expression are necessary for S1P to induce the peripheral biomechanical forces involved in EC barrier enhancement.[30,58-60] Consistent with depiction of reduced lamellipodia protrusion velocity (Fig 4C) and reduced barrier protection (Fig 4D, E) in EC with cortactin S484N, EC overexpressing cortactin S484N exhibit decreased elastic modulus responses within lamellipodia following thrombin (1 U/ml) or S1P (1 μM; Fig 4F, G), indicative of abnormal cytoskeletal rearrangement. In these experiments, live HPAEC were transfected with EGFP-labeled WT cortactin, EGFP-S484N cortactin, or EGFP plasmid control, and peripheral cell regions next selected to assess lamellipodia force dynamics over time, initially in response to thrombin, to model inflammatory agonist-induced permeability, then followed by S1P treatment, to model EC barrier recovery (Fig 4G). Thrombin induced a

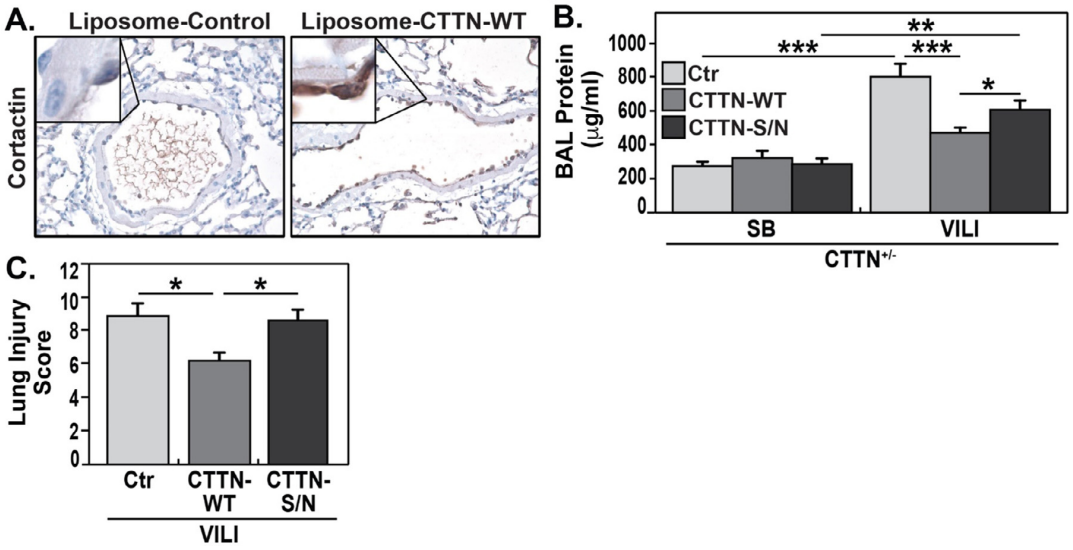

Fig 7. Endothelial expression of *CTTN* S484N SNP exacerbates lung permeability responses in VILI-exposed mice. Plasmids encoding c-myc-tagged WT or SNP S484N (S/N) cortactin were combined with ACE Ab-liposomes and then infused into cortactin heterozygous ($CTTN^{+/-}$) mice via the internal jugular vein. **A)** Histological lung specimens (collected 24 hrs after liposome administration) were analyzed by IHC for the c-myc tag. Brown staining (inset) indicates presence of the c-myc-tagged construct in the vascular endothelium, which is not present in control mice (treated with liposomes containing empty vector). **B)** Bronchoalveolar lavage (BAL) protein levels were measured 4 hrs after ventilation (30 ml/kg; VILI model) or in spontaneous breathing (SB) mice that had received ACE antibody-conjugated liposome delivery of plasmids (Ctr, WT, or S/N). **C)** Histological injury scores of lungs from VILI mice treated with ACE antibody-conjugated liposomes containing plasmids (Ctr, WT, or S/N). N = 3−7 mice per group. *$P < 0.05$, ** $P < 0.01$, *** $P < 0.001$.

rapid decline of peripheral elastic modulus in WT cortactin and EGFP-control EC, however, responses in S484N cortactin EC were delayed and less robust, demonstrating abnormal cytoskeletal rearrangement. EC expressing WT cortactin began to more quickly recover to baseline even before S1P addition when compared to EGFP control EC, consistent with an important barrier-promoting role for WT cortactin. However, EC expressing S484N cortactin failed to increase peripheral elastic properties in response to S1P and failed to return to baseline values, further highlighting the negative impact of the S484N cortactin SNP on EC cytoskeletal structure and barrier function.

Reduced cortactin S484N-nmMLCK interaction in agonist-stimulated EC. Cortactin interaction with nmMLCK is increased by tyrosine phosphorylation of either nmMLCK or cortactin,[32,33] an event critical to S1P-induced EC barrier enhancement.[29,32,33,72] The effect of the S484N SNP on cortactin-nmMLCK interaction was investigated in EC transfected with a Flag-tagged nmMLCK construct and c-myc-tagged cortactin constructs expressing either the WT or the cortactin S484N protein. Co-immunoprecipitation studies in EC stimulated with S1P (1 μM, 10 minutes) utilizing either immunoprecipitation of nmMLCK (Fig 5A) or cortactin (Fig 5B), demonstrated an increased cortactin-nmMLCK binding interaction with WT cortactin but not with cortactin S484N.

We previously demonstrated that Src kinase-mediated phosphorylation of either cortactin or nmMLCK protein increases nmMLCK and cortactin binding.[32] Recombinant GST-tagged cortactin and Flag-tagged nmMLCK proteins were incubated with recombinant Src kinase for 5 minutes, and GST-cortactin then isolated by antibody binding. Subsequent western blots demonstrate a significant increase in nmMLCK binding to Src-phosphorylated WT GST-cortactin compared to Src-phosphorylated S484N (0.42 ± 0.11 vs WT). No differences in nmMLCK-cortactin interactions were observed at baseline (Fig 5C, D).

Cortactin expression modulates preclinical ARDS in mice. Next, we explored the influence of cortactin S484N in the development of acute lung injury *in vivo* employing $CTTN^{+/-}$ heterozygous mice that express ~50% less cortactin in lung tissues compared to wild-type (WT; data not shown). $CTTN^{+/-}$ and WT mice were exposed to either LPS or VILI, established models of preclinical ARDS.[64,73] As seen in Fig 6A, B, WT mice exposed to intratracheal LPS exhibit increased

bronchoalveolar lavage (BAL) total protein levels (1316 ± 200 μg/ml) and cell counts (4.38 ± 0.67 × 10^6) indicating increased alveolo-capillary permeability and inflammation which, importantly, were significantly augmented in LPS-treated *CTTN*$^{+/-}$ mice (1808 ± 142 μg/ml and 6.97 ± 0.99 × 10^6). Complementary histologic examination of H&E lung tissue staining confirmed LPS-induced edema and inflammatory cell infiltration into the lungs of WT mice, with these changes more pronounced in *CTTN*$^{+/-}$ mice (Fig 6C). Neutrophil recruitment into the alveolar space was quantified after differential counting of BAL cells with marked increases in neutrophil counts in *CTTN+/-* mice treated with LPS) compared to WT (6.60 ± 0.90 × 10^6 vs 3.19 ± 0.50 × 10^6; Fig 6D). Consistent with these findings, we observed that *CTTN*$^{+/-}$ mice exposed to the clinically relevant model of murine VILI, exhibit significantly increased BAL protein (767 ± 42 μg/ml vs 541 ± 58 μg/ml) and total cell counts (1.95 ± 0.13 × 10^6 vs 1.14 ± 0.07 × 10^6) compared to WT mice (Fig 6E, F). Taken together, these data provide strong evidence that reduced cortactin expression is associated with increased levels of lung injury and indicate that cortactin exerts a protective role against inflammatory lung injury *in vivo*.

Cortactin S484N exacerbates vascular leak in ventilator-induced lung injury. To confirm *in vivo* the effects of the cortactin S484N protein on vascular barrier regulation, *CTTN*$^{+/-}$ mice, shown in Fig 6 to be more susceptible to acute lung injury, were injected IV with cortactin constructs (WT or S484N) encargoed within ACE antibody-tagged liposomes[65] to reconstitute cortactin expression specifically in vascular EC. Successful delivery of cortactin constructs in an EC-specific manner to the lung vasculature was confirmed by immunohistochemistry (Fig 7A). *CTTN*$^{+/-}$ mice with liposome delivery of exogenous WT or S484N cortactin were intubated and subjected to VILI (30 ml/kg, 4 hours). Compared to spontaneously breathing animals, VILI-exposed *CTTN*$^{+/-}$ mice receiving control liposomes demonstrate substantially increased levels of BAL protein (808 ± 68 μg/ml; Fig 7B). Importantly, delivery of WT cortactin to the endothelium of *CTTN*$^{+/-}$ animals significantly reduced BAL protein (474 ± 29 μg/ml), while delivery of the cortactin S484N transgene resulted in less significant protection (613 ± 48 μg/ml; Fig 7B). The histologic lung injury scores were significantly decreased in VILI mice receiving WT cortactin compared to controls (6.2 ± 0.4 vs 8.9 ± 0.6), while animals receiving the cortactin S484N transgene exhibited no protection (8.7 ± 0.5; Fig 7C).

DISCUSSION

Inflammatory lung injury such as ARDS results in high mortality and occurs frequently in critically ill patients suffering from severe infections (eg, SARS-CoV-2), trauma, VILI, and other inflammatory conditions.[2,6,63,74] Racial and ethnic disparities in ARDS risk and mortality have been reported in multiple epidemiologic studies.[10,75-78] Black individuals suffer worse healthcare outcomes in the US than non-Hispanic whites, and the COVID-19 pandemic has exacerbated these health disparities.[7,8] Recent data from the CDC indicate that patients of African descent in the US are 2.9 times more likely to be hospitalized with COVID-19 infection than white non-Hispanics, are 1.9 times more likely to die from severe disease,[79] and exhibit higher risk for developing ARDS.[11] Although societal issues contribute to this increased risk, valuable additional insights can be gained through characterization of genetic biomarkers associated with ARDS susceptibility and severity.[9,12]

Potential candidate genes of interest may be identified through their known participation in the pathobiology that underlies ARDS. In these critically ill patients, respiratory failure occurs due to inflammation-induced disruption of the pulmonary vascular EC barrier and subsequent alveolar flooding and hypoxemia. EC barrier function is determined in large part by the structure and arrangement of its cellular cytoskeleton.[22,28] Given the importance of cytoskeletal proteins in determining lung vascular permeability, we hypothesized that variants in genes encoding critical cytoskeletal proteins may be associated with ARDS risk. Prior work has validated this approach and identified multiple polymorphisms (SNPs) in cytoskeletal- and EC permeability-regulating genes that may have utility as biomarkers in ARDS.[12] Examples include *NAMPT* (encoding nicotinamide phosphoribosyltransferase),[13,14] *MYLK* (encoding nmMLCK),[15-17] *GADD45a* (growth arrest and DNA damage-inducible protein),[18] *S1P3* (the sphingosine-1-phosphate receptor 3),[19] *SELPLG* (P-selectin glycoprotein ligand 1),[20] and *FLT1* (encoding vascular endothelial growth factor receptor 1 or VEGF1).[80] Several SNPs in *MYLK* confer differential ARDS risk in those of African descent,[15-17,81] which highlights the potential of this approach to provide new insights into health disparities in ARDS.

The current study significantly advances prior work by characterizing a *CTTN* SNP as a novel genetic risk variant for increasing severity of inflammatory injury in Blacks and by providing the functional basis for this increased risk. Cortactin is an actin-binding and cytoskeletal protein that mediates EC cytoskeletal

rearrangements that regulate lung vascular barrier function.[28-33,37,45] The human *CTTN* gene is located at chromosome position 11q13.3 and contains 20 exons. Despite being a putative oncogene[37,82] and critical cytoskeletal effector, relatively little detail is known about how *CTTN* variants are linked to human disease. We previously reported a significant association between an intronic *CTTN* SNP (rs3802780) and severe asthma with independent and additive effects of *CTTN* and *MYLK* risk variants for severe asthma susceptibility in patients of African descent.[47] The *CTTN* rs56162978A polymorphism is rare in European descent subjects (<0.1%) but with a much higher allelic frequency in African descent subjects (16%). We characterized the potential association of the rs56162978 SNP with clinical outcomes/severity in two separate cohorts of Black subjects with inflammatory injury. In the first validation group of 725 Black patients with sepsis, a primary risk factor for developing ARDS, the rs56162978 SNP was associated with increased risk of 30-day sepsis mortality (Table 3). In a second validation cohort in Black patients, we examined rs56162978 SNP association in sickle cell disease (SCD) subjects who frequently suffer from the acute chest syndrome (ACS), a form of ARDS and a major source of morbidity and mortality. ACS is the second leading cause of hospitalization and the most common cause of death in adult SCD patients.[67] Unlike ARDS, only 15% of patients presenting with ACS require mechanical ventilation, and ACS carries an overall 3% mortality.[68] In our cohort of SCD patients, the *CTTN* SNP rs56162978 was significantly associated with increased risk of developing ACS, with an even stronger association observed with ACS severity (episodes requiring mechanical ventilation, Fig 1B, C). These data are highly novel as few SNPs have been reported to associate with ACS.[83-85] Together, these studies in 2 cohorts of Black subjects, support a genetic basis for the increased health disparities observed in Black patients with critical illnesses.

To provide new mechanistic insights into a potential role for cortactin in ACS/ARDS pathophysiology, we directly examined the functionality of the *CTTN* S484N SNP in lung EC barrier regulation. Increased lung vascular permeability, a cardinal feature of ARDS, represents an imbalance between barrier-disrupting cellular contractile forces and barrier-protective cell-cell and cell-matrix tethering forces, with both competing forces intimately linked to the actin-based EC cytoskeleton by a variety of actin-binding proteins.[22,28] EC contractile force is generated via actomyosin interactions catalyzed by the MLC phosphorylation activity of nmMLCK.[86] Recovery from inflammatory edema involves increased MLC phosphorylation at the cell periphery, enhanced by potent barrier-enhancing agents such as S1P,[29,87,88] which evokes cell spreading, flattening, and other changes to strengthen the cortical actin ring and its connections to cell-tethering sites. Our prior studies have identified a critical role for the interaction of nmMLCK with cortactin in S1P-induced EC barrier enhancement.[29,33]

The amino acid structure of cortactin is ideally suited for integrating multiple signals at sites of dynamic actin rearrangement to restore EC barrier integrity and reduce permeability. Cortactin contains an N-terminal acidic region (NTA) that stimulates actin polymerization by the Arp2/3 complex (AA #1-90), a tandem repeat site for actin binding (AA #91-326), a proline-rich area containing serine and tyrosine phosphorylation sites (AA #401-495), and a C-terminal SH3 domain (#496-546) through which it interacts with multiple cytoskeletal proteins (Fig 1).[35,37] Tyrosine phosphorylation of cortactin by multiple kinases, such as Src, c-Abl/Arg, Fer, and Fyn, is increased at 3 key residues (Y^{421}, Y^{466} and Y^{482} in mouse cortactin [Y^{486} in human cortactin]) after many stimuli associated with cytoskeletal rearrangement (eg, S1P, EGF, thrombin, integrin activation, shear stress) and integrates multiple signaling cascades with the actin cytoskeleton.[33,38,39] We have reported that phosphorylation of cortactin by Src or c-Abl increases its association with nmMLCK and regulates Arp2/3-mediated actin polymerization.[29,32,33] Importantly, in the current study we show that the S484N SNP decreases phosphorylation at the critical Y^{486} phosphorylation signaling site (Fig. 2 and 3), suggesting alterations in cortactin function via effects on this post-translational modification. Additional functional studies in human lung EC demonstrated significant inhibitory effects of the S484N SNP on peripheral cytoskeletal protrusions (kymography), barrier recovery following thrombin- or LPS-induced EC permeability (ECIS), and peripheral elastic properties and force generation (AFM; Fig 4). These new data complement and substantially advance the mechanistic understanding of our previous observations: (a) AFM studies that showed c-Abl signaling and cortactin expression are necessary for S1P to induce the peripheral biomechanical forces involved in EC barrier enhancement,[30,58-60] and (b) lung EC expressing the S484N cortactin variant have impaired wound closure and cell locomotion.[31]

The interaction between cortactin and nmMLCK provides a direct link between the effects of S484N on actin cytoskeletal structure and force generation that result in delayed EC barrier recovery. Cortactin is unique among cytoskeletal regulatory proteins in the ability to both stabilize static actin structures and

stimulate dynamic rearrangements of peripheral actin. It interacts with several cytoskeletal effector proteins through its C-terminal SH3 domain to regulate actin polymerization and force generation, including nmMLCK.[29,32,33,35,37,89] Cortactin facilitates nmMLCK-actin binding through an interaction at two proline rich sites in the latter molecule which is induced by Src kinase activation.[32] Inhibition of cortactin-MLCK interaction reduces maximal S1P-induced barrier enhancement in cultured ECs[90] and cortactin and nmMLCK demonstrate increased co-localization within lamellipodia following S1P.[72] Interestingly, nmMLCK fragments containing mutations of critical proline residues within the putative cortactin binding sites exhibit an increased association with cortactin, while these same mutations in the full-length constructs showed increased kinase activity.[54] Increased stress fibers and membrane retractions were also observed in ECs transfected with the proline-deficient nmMLCK[54] suggesting a more barrier-disruptive phenotype. NMR spectroscopy and molecular modeling analysis of ARDS-associated SNPs in the gene encoding nmMLCK (*MYLK*) identified alterations in protein structure and increased accessibility of key proline-rich loops, which may account for observed differences in cortactin binding between nmMLCK isoforms.[91] Moreover, these same *MYLK* SNPs reduce nmMLCK tyrosine phosphorylation, peripheral localization, and lamellipodia responses after S1P in lung EC,[46] which are all cytoskeletal events associated with permeability changes. Collectively, these studies provide convincing evidence for the importance of the cortactin-nmMLCK interaction in regulating processes that determine EC barrier integrity. The current study identified the cortactin S484N to disrupt cortactin association with nmMLCK (Fig 5), a protein-protein interaction that enhances EC barrier function.

In vivo studies provide further support that the *CTTN* rs56162978 SNP is fundamentally involved in functional regulation of pulmonary vascular integrity and permeability. Prior studies utilizing a global *CTTN* knockout (exon deletion) reported that homozygotes have increased intradermal permeability after histamine injection[92] and higher gastrointestinal permeability in a colitis model.[93] We utilized a murine mouse line where *CTTN* homozygous KOs have embryonic lethality but heterozygous mice develop normally, are fertile, and have no obvious pulmonary phenotype at baseline.[61] Two preclinical models of ARDS were employed to characterize the effects of cortactin expression and Ser484Asn *in vivo*—intratracheal LPS and VILI.[63,94] *CTTN*+/- mice injured by either high tidal mechanical ventilation or LPS, exhibit higher inflammatory responses (BAL WBC levels) and increased BAL protein as a marker of vascular leak, compared to WT mice (Fig 6), indicating that cortactin deficiency increases susceptibility to preclinical ARDS. We next employed ACE-linked liposomes to selectively restore cortactin expression in lung endothelium[65] by "add back" of either WT or S484N cortactin. Consistent with an EC barrier-protective role of cortactin, $CTTN^{+/-}$ mice in which WT protein expression was augmented by ACE-linked liposomes exhibited significant reductions in VILI-induced BAL protein and histologic lung injury score (Fig 7). Most importantly, the protective effects of cortactin augmentation were lost in mice receiving liposomes containing the S484N protein (Fig 7). These data strongly support a functional role for the rs56162978 SNP in modulating lung EC barrier integrity and EC barrier recovery responses to increase risk and severity of pathologic inflammatory states modulating vascular integrity.

We recognize several limitations of our study, including the modest size of our Black subject cohorts. Clearly, these observations would be further strengthened by further study in larger patient groups enriched in those of African descent, including COVID-19 ARDS patients. Although a 16% minor allele frequency is not rare, the number of homozygous recessive subjects is low, and low frequency events may produce unstable risk effect estimates. However, as a coding SNP with proven functional consequences, we believe the association with sepsis mortality among homozygous recessive carriers is significant. Another limitation was the use of lung EC containing endogenous cortactin as well as overexpressed WT or S484N cortactin. Thus a portion of S484N variant effects may be obscured. We attempted to address this limitation by confirmatory barrier function studies using human aortic EC genetically edited by CRISPR to express only WT cortactin, or only the S484N alleles. Finally, the $CTTN^{+/-}$ mice used in this study are globally deficient for cortactin in all cell types, increasing the likelihood that a portion of the effects noted in the preclinical models may reflect the absence of cortactin in cell types other than lung EC, such as epithelium or migrating leukocytes. Our ACE-antibody-linked liposome experiments support the hypothesis that lung EC expression of cortactin plays a primary role in ARDS, however, it remains possible that cortactin expression in other cell types also has functional importance.

In summary, our data demonstrate that the human *CTTN* rs56162978 SNP, encoding a S484N protein variant, is associated with risk of inflammatory lung injury in patients of African descent. The substitution of asparagine at Ser484 adversely affects human lung EC cytoskeletal signaling and barrier function *in vitro*, and exacerbates the severity of inflammatory injury in

preclinical models of ARDS in mice *in vivo*. These results strongly support a critical role for cortactin in maintenance of the pulmonary vascular barrier integrity and improves our mechanistic understanding of genetic susceptibility to ARDS and inflammatory injury. This work advances our understanding of health disparities in Black patients with ARDS and may improve risk stratification and therapeutic targeting in future studies.

ACKNOWLEDGMENTS

Conflicts of interest: All authors have read the journal's policy on disclosure of potential conflicts of interest and no financial or personal relationship with organizations that could potentially be perceived as influencing the described research were identified.

All authors have read the journal's authorship agreement. This study was funded by NIH K08 HL135318 (P.B.), K08 HL141623 (C.B.), P01 HL126609 (J.G.N.G.), R01 HL088144 (S.M.D.), R01 HL133059 (S.M.D.), and R01s HL137006 and HL137915 (N.J.M). We thank Dr. Xi Zhan for generously providing the *CTTN*$^{+/-}$ mice, and Dr. Roberto Machado for SCD patient cohort organization and analysis.

REFERENCES

1. Matthay MA, Ware LB, Zimmerman GA. The acute respiratory distress syndrome. J Clin Invest 2012;122:2731–40.
2. Thompson BT, Chambers RC, Liu KD. Acute Respiratory Distress Syndrome. N Engl J Med 2017;377:562–72.
3. Pons S, Fodil S, Azoulay E, Zafrani L. The vascular endothelium: the cornerstone of organ dysfunction in severe SARS-CoV-2 infection. Crit Care 2020;24:353.
4. Short KR, Kroeze E, Fouchier RAM, Kuiken T. Pathogenesis of influenza-induced acute respiratory distress syndrome. Lancet Infect Dis 2014;14:57–69.
5. Meduri GU, Reddy RC, Stanley T, El-Zeky F. Pneumonia in acute respiratory distress syndrome. A prospective evaluation of bilateral bronchoscopic sampling. Am J Respir Crit Care Med 1998;158:870–5.
6. Grasselli G, Tonetti T, Protti A, et al. Pathophysiology of COVID-19-associated acute respiratory distress syndrome: a multicentre prospective observational study. Lancet Respir Med 2020;8:1201–8.
7. Bhargava A, Sharma M, Akagi E, Szpunar SM, Saravolatz L. Predictors for in-hospital mortality from coronavirus disease 2019 (COVID-19) infection among adults aged 18-65 years. Infect Control Hosp Epidemiol 2020:1–4.
8. Chowkwanyun M, Reed AL Jr.. Racial Health Disparities and Covid-19 - caution and context. N Engl J Med 2020;383:201–3.
9. Garcia JG, Sznajder JI. Healthcare disparities in patients with acute respiratory distress syndrome. Toward equity. Am J Respir Crit Care Med 2013;188:631–2.
10. Bime C, Poongkunran C, Borgstrom M, et al. Racial differences in mortality from severe acute respiratory failure in the United States, 2008-2012. Ann Am Thorac Soc 2016;13:2184–9.
11. Cates J, Lucero-Obusan C, Dahl RM, et al. Risk for in-hospital complications associated with covid-19 and influenza - Veterans Health Administration, United States, October 1, 2018-May 31, 2020. MMWR Morb Mortal Wkly Rep 2020;69:1528–34.
12. Lynn H, Sun X, Casanova N, Gonzales-Garay M, Bime C, Garcia JGN. Genomic and genetic approaches to deciphering acute respiratory distress syndrome risk and mortality. Antioxid Redox Signal 2019;31:1027–52.
13. Ye SQ, Simon BA, Maloney JP, et al. Pre-B-cell colony-enhancing factor as a potential novel biomarker in acute lung injury. Am J Respir Crit Care Med 2005;171:361–70.
14. Sun X, Elangovan VR, Mapes B, et al. The NAMPT promoter is regulated by mechanical stress, signal transducer and activator of transcription 5, and acute respiratory distress syndrome-associated genetic variants. Am J Respir Cell Mol Biol 2014;51:660–7.
15. Mascarenhas JB, Tchourbanov AY, Fan H, Danilov SM, Wang T, Garcia JG. Mechanical stress and single nucleotide variants regulate alternative splicing of the MYLK Gene. Am J Respir Cell Mol Biol 2017;56:29–37.
16. Gao L, Grant A, Halder I, et al. Novel polymorphisms in the myosin light chain kinase gene confer risk for acute lung injury. Am J Respir Cell Mol Biol 2006;34:487–95.
17. Christie JD, Ma SF, Aplenc R, et al. Variation in the myosin light chain kinase gene is associated with development of acute lung injury after major trauma. Crit Care Med 2008;36:2794–800.
18. Meyer NJ, Huang Y, Singleton PA, et al. GADD45a is a novel candidate gene in inflammatory lung injury via influences on Akt signaling. FASEB J 2009;23:1325–37.
19. Sun X, Ma SF, Wade MS, et al. Functional promoter variants in sphingosine 1-phosphate receptor 3 associate with susceptibility to sepsis-associated acute respiratory distress syndrome. Am J Physiol Lung Cell Mol Physiol 2013;305:L467–77.
20. Bime C, Pouladi N, Sammani S, et al. Genome-wide association study in African Americans with acute respiratory distress syndrome identifies the Selectin P Ligand Gene as a Risk Factor. Am J Respir Crit Care Med 2018;197:1421–32.
21. Bhattacharya J, Matthay MA. Regulation and repair of the alveolar-capillary barrier in acute lung injury. Ann Review Physiol 2013;75:593–615.
22. Dudek SM, Garcia JG. Cytoskeletal regulation of pulmonary vascular permeability. JApplPhysiol 2001;91:1487–500.
23. Huppert LA, Matthay MA, Ware LB. Pathogenesis of Acute Respiratory Distress Syndrome. Semin Respir Crit Care Med 2019;40:31–9.
24. Simmons S, Erfinanda L, Bartz C, Kuebler WM. Novel mechanisms regulating endothelial barrier function in the pulmonary microcirculation. J Physiol 2019;597:997–1021.
25. Ackermann M, Verleden SE, Kuehnel M, et al. Pulmonary vascular endothelialitis, thrombosis, and angiogenesis in Covid-19. N Engl J Med 2020;383:120–8.
26. Bime C, Casanova NG, Nikolich-Zugich J, Knox KS, Camp SM, Garcia JGN. Strategies to DAMPen COVID-19-mediated lung and systemic inflammation and vascular injury. Transl Res 2021;232:37–48.
27. Fox SE, Akmatbekov A, Harbert JL, Li G, Quincy Brown J, Vander Heide RS. Pulmonary and cardiac pathology in African American patients with COVID-19: an autopsy series from New Orleans. Lancet Respir Med 2020;8:681–6.
28. Belvitch P, Htwe YM, Brown ME, Dudek S. Cortical Actin Dynamics in Endothelial Permeability. Curr Top Membr 2018;82:141–95.

29. Dudek SM, Jacobson JR, Chiang ET, et al. Pulmonary endothelial cell barrier enhancement by sphingosine 1-phosphate: roles for cortactin and myosin light chain kinase. J Biol Chem 2004;279:24692–700.
30. Arce FT, Whitlock JL, Birukova AA, et al. Regulation of the micromechanical properties of pulmonary endothelium by S1P and thrombin: role of cortactin. Biophys J 2008;95:886–94.
31. Choi S, Camp SM, Dan A, Garcia JG, Dudek SM, Leckband DE. A genetic variant of cortactin linked to acute lung injury impairs lamellipodia dynamics and endothelial wound healing. Am J Physiol Lung Cell Mol Physiol 2015;309:L983–94.
32. Dudek SM, Birukov KG, Zhan X, Garcia JG. Novel interaction of cortactin with endothelial cell myosin light chain kinase. Biochem Biophys Res Commun 2002;298:511–9.
33. Dudek SM, Chiang ET, Camp SM, et al. Abl tyrosine kinase phosphorylates nonmuscle Myosin light chain kinase to regulate endothelial barrier function. Mol Biol Cell 2010;21:4042–56.
34. Ammer AG, Weed SA. Cortactin branches out: roles in regulating protrusive actin dynamics. Cell Motility Cytoskeleton 2008;65:687–707.
35. Cosen-Binker LI, Kapus A. Cortactin: the gray eminence of the cytoskeleton. Physiology (Bethesda) 2006;21:352–61.
36. Camp SM, Bittman R, Chiang ET, et al. Synthetic analogs of FTY720 [2-amino-2-(2-[4-octylphenyl]ethyl)-1,3-propanediol] differentially regulate pulmonary vascular permeability in vivo and in vitro. J Pharmacol Exp Therapeut 2009;331:54–64.
37. Schnoor M, Stradal TE, Cortactin Rottner K. Cell Functions of A Multifaceted Actin-Binding Protein. Trends Cell Biol 2018;28:79–98.
38. Boyle SN, Michaud GA, Schweitzer B, Predki PF, Koleske AJ. A critical role for cortactin phosphorylation by Abl-family kinases in PDGF-induced dorsal-wave formation. Curr Biol 2007;17:445–51.
39. Lua BL, Low BC. Cortactin phosphorylation as a switch for actin cytoskeletal network and cell dynamics control. FEBS Lett 2005;579:577–85.
40. Huang C, Liu J, Haudenschild CC, Zhan X. The role of tyrosine phosphorylation of cortactin in the locomotion of endothelial cells. J Biol Chem 1998;273:25770–6.
41. Jacobson JR, Dudek SM, Singleton PA, Kolosova IA, Verin AD, Garcia JG. Endothelial cell barrier enhancement by ATP is mediated by the small GTPase Rac and cortactin. Am J Physiol Lung Cell Mol Physiol 2006;291:L289–95.
42. Singleton PA, Salgia R, Moreno-Vinasco L, et al. CD44 regulates hepatocyte growth factor-mediated vascular integrity. Role of c-Met, Tiam1/Rac1, dynamin 2, and cortactin. J Biol Chem 2007;282:30643–57.
43. Zhao J, Singleton PA, Brown ME, Dudek SM, Garcia JG. Phosphotyrosine protein dynamics in cell membrane rafts of sphingosine-1-phosphate-stimulated human endothelium: role in barrier enhancement. Cell Signal 2009;21:1945–60.
44. Schnoor M, Lai FP, Zarbock A, et al. Cortactin deficiency is associated with reduced neutrophil recruitment but increased vascular permeability in vivo. The Journal of experimental medicine 2011;208:1721–35.
45. Garcia Ponce A, Citalan Madrid AF, Vargas Robles H, et al. Loss of cortactin causes endothelial barrier dysfunction via disturbed adrenomedullin secretion and actomyosin contractility. Sci Rep 2016;6:29003.
46. Wang T, Brown ME, Kelly GT, et al. Myosin light chain kinase (MYLK) coding polymorphisms modulate human lung endothelial cell barrier responses via altered tyrosine phosphorylation, spatial localization, and lamellipodial protrusions. Pulm Circ 2018;8:2045894018764171.
47. Ma SF, Flores C, Wade MS, et al. A common cortactin gene variation confers differential susceptibility to severe asthma. Genetic Epidemiol 2008;32:757–66.
48. Desai AA, Lei Z, Bahroos N, et al. Association of circulating transcriptomic profiles with mortality in sickle cell disease. Blood 2017;129:3009–16.
49. Desai AA, Zhou T, Ahmad H, et al. A novel molecular signature for elevated tricuspid regurgitation velocity in sickle cell disease. Am J Respir Crit Care Med 2012;186:359–68.
50. Gupta A, Fei YD, Kim TY, et al. IL-18 mediates sickle cell cardiomyopathy and ventricular arrhythmias. Blood 2021;137:1208–18.
51. Reilly JP, Meyer NJ, Shashaty MG, et al. The ABO histo-blood group, endothelial activation, and acute respiratory distress syndrome risk in critical illness. J Clin Invest 2021:131.
52. Reilly JP, Wang F, Jones TK, et al. Plasma angiopoietin-2 as a potential causal marker in sepsis-associated ARDS development: evidence from Mendelian randomization and mediation analysis. Intensive Care Med 2018;44:1849–58.
53. Rizzo AN, Belvitch P, Demeritte R, Garcia JGN, Letsiou E, Dudek SM. Arg mediates LPS-induced disruption of the pulmonary endothelial barrier. Vascul Pharmacol 2020;128-129:106677.
54. Belvitch P, Adyshev D, Elangovan VR, et al. Proline-rich region of non-muscle myosin light chain kinase modulates kinase activity and endothelial cytoskeletal dynamics. Microvasc Res 2014;95:94–102.
55. Yi K, Unruh JR, Deng M, Slaughter BD, Rubinstein B, Li R. Dynamic maintenance of asymmetric meiotic spindle position through Arp2/3-complex-driven cytoplasmic streaming in mouse oocytes. Nat Cell Biol 2011;13:1252–8.
56. Ott C, Lippincott-Schwartz J. Visualization of live primary cilia dynamics using fluorescence microscopy. Curr Protoc Cell Biol 2012:Chapter 4: Unit 4 26.
57. Doggett TM, Breslin JW. Study of the actin cytoskeleton in live endothelial cells expressing GFP-actin. J of Visual Exp 2011.
58. Wang X, Bleher R, Brown ME, et al. Nano-biomechanical study of spatio-temporal cytoskeleton rearrangements that determine subcellular mechanical properties and endothelial permeability. Sci Rep 2015;5:11097.
59. Wang X, Bleher R, Wang L, et al. Imatinib alters agonists-mediated cytoskeletal biomechanics in lung endothelium. Sci Rep 2017;7:14152.
60. Wang X, Wang L, Garcia JGN, Dudek SM, Shekhawat GS, Dravid VP. The significant role of c-Abl kinase in barrier altering agonists-mediated cytoskeletal biomechanics. Sci Rep 2018;8:1002.
61. Yu D, Zhang H, Blanpied TA, Smith E, Zhan X. Cortactin is implicated in murine zygotic development. Exp Cell Res 2010;316:848–58.
62. Fan E, Brodie D, Slutsky AS. Acute Respiratory Distress Syndrome: advances in diagnosis and treatment. JAMA 2018;319:698–710.
63. Slutsky AS, Ranieri VM. Ventilator-induced lung injury. N Engl J Med 2013;369:2126–36.
64. Letsiou E, Rizzo AN, Sammani S, et al. Differential and opposing effects of imatinib on LPS- and ventilator-induced lung injury. Am J Physiol 2015;308:L259–69.
65. Mirzapoiazova T, Moitra J, Moreno-Vinasco L, et al. Non-muscle myosin light chain kinase isoform is a viable molecular target in acute inflammatory lung injury. Am J Respir Cell Mol Biol 2011;44:40–52.
66. Genomes Project C, Auton A, Brooks LD, et al. A global reference for human genetic variation. Nature 2015;526:68–74.

67. Paul RN, Castro OL, Aggarwal A, Oneal PA. Acute chest syndrome: sickle cell disease. Eur J Haematol 2011;87:191–207.
68. Vichinsky EP, Neumayr LD, Earles AN, et al. Causes and outcomes of the acute chest syndrome in sickle cell disease. National Acute Chest Syndrome Study Group. N Engl J Med 2000;342:1855–65.
69. Bryce NS, Clark ES, Leysath JL, Currie JD, Webb DJ, Weaver AM. Cortactin promotes cell motility by enhancing lamellipodial persistence. Curr Biol 2005;15:1276–85.
70. Giannone G, Dubin-Thaler BJ, Rossier O, et al. Lamellipodial actin mechanically links myosin activity with adhesion-site formation. Cell 2007;128:561–75.
71. Kronlage C, Schäfer-Herte M, Böning D, Oberleithner H, Fels J. Feeling for filaments: quantification of the cortical actin web in live vascular endothelium. Biophys J 2015;109:687–98.
72. Brown M, Adyshev D, Bindokas V, Moitra J, Garcia JG, Dudek SM. Quantitative distribution and colocalization of non-muscle myosin light chain kinase isoforms and cortactin in human lung endothelium. Microvasc Res 2010;80:75–88.
73. Matute-Bello G, Downey G, Moore BB, et al. Acute Lung Injury in Animals Study G. An official American Thoracic Society workshop report: features and measurements of experimental acute lung injury in animals. Am J Respir Cell Mol Biol 2011;44:725–38.
74. Bellani G, Laffey JG, Pham T, et al. Epidemiology, patterns of care, and mortality for patients with acute respiratory distress syndrome in intensive care units in 50 countries. JAMA 2016;315:788–800.
75. Cooke CR, Erickson SE, Eisner MD, Martin GS. Trends in the incidence of noncardiogenic acute respiratory failure: the role of race. Crit Care Med 2012;40:1532–8.
76. Erickson SE, Shlipak MG, Martin GS, et al. National Institutes of Health National Heart L, Blood Institute Acute Respiratory Distress Syndrome N. Racial and ethnic disparities in mortality from acute lung injury. Crit Care Med 2009;37:1–6.
77. Lemos-Filho LB, Mikkelsen ME, Martin GS, et al. Injury Trials Group: Lung Injury Prevention Study I. Sex, race, and the development of acute lung injury. Chest 2013;143:901–9.
78. Moss M, Mannino DM. Race and gender differences in acute respiratory distress syndrome deaths in the United States: an analysis of multiple-cause mortality data (1979- 1996). Crit Care Med 2002;30:1679–85.
79. National Center for Immunization and Respiratory Diseases (NCIRD) DoVD. Risk for COVID-19 Infection, Hospitalization, and Death By Race/Ethnicity 2021:[Website]July 16, 2021 [cited 2021 August 10]. Available from https://www.cdc.gov/coronavirus/2019-ncov/covid-data/investigations-discovery/hospitalization-death-by-race-ethnicity.html.
80. Guillen-Guio B, Lorenzo-Salazar JM, Ma SF, et al. Sepsis-associated acute respiratory distress syndrome in individuals of European ancestry: a genome-wide association study. Lancet Respir Med 2020;8:258–66.
81. Szilagyi KL, Liu C, Zhang X, et al. Epigenetic contribution of the myosin light chain kinase gene to the risk for acute respiratory distress syndrome. Transl Res 2017;180:12–21.
82. Kirkbride KC, Sung BH, Sinha S, Weaver AM. Cortactin: a multifunctional regulator of cellular invasiveness. Cell Adhesion Migration 2011;5:187–98.
83. Driss A, Asare KO, Hibbert JM, Gee BE, Adamkiewicz TV, Stiles JK. Sickle cell disease in the post genomic era: a monogenic disease with a polygenic phenotype. Genomics insights 2009;2009:23–48.
84. Bean CJ, Boulet SL, Yang G, et al. Acute chest syndrome is associated with single nucleotide polymorphism-defined beta globin cluster haplotype in children with sickle cell anaemia. Br J Haematol 2013;163:268–76.
85. Galarneau G, Coady S, Garrett ME, et al. Gene-centric association study of acute chest syndrome and painful crisis in sickle cell disease patients. Blood 2013;122:434–42.
86. Goeckeler ZM, Wysolmerski RB. Myosin light chain kinase-regulated endothelial cell contraction: the relationship between isometric tension, actin polymerization, and myosin phosphorylation. J Cell Biol 1995;130:613–27.
87. Garcia JG, Liu F, Verin AD, et al. Sphingosine 1-phosphate promotes endothelial cell barrier integrity by Edg-dependent cytoskeletal rearrangement. J Clin Invest 2001;108:689–701.
88. Maeng YS, Maharjan S, Kim JH, et al. Rk1, a ginsenoside, is a new blocker of vascular leakage acting through actin structure remodeling. PloS one 2013;8:e68659.
89. Zarrinpar A, Bhattacharyya RP, Lim WA. The structure and function of proline recognition domains. Sci STKE 2003;2003:RE8.
90. Dudek SM, Jacobson JR, Chiang ET, et al. Pulmonary endothelial cell barrier enhancement by sphingosine 1-phosphate: roles for cortactin and myosin light chain kinase. J Biol Chem 2004;279:24692–700.
91. Shen K, Ramirez B, Mapes B, et al. Structure-function analysis of the non-muscle myosin light chain kinase (nmMLCK) Isoform by NMR spectroscopy and molecular modeling: influence of MYLK variants. PloS One 2015;10:e0130515.
92. Mitra S, Sammani S, Wang T, et al. Role of growth arrest and DNA damage-inducible alpha in Akt phosphorylation and ubiquitination after mechanical stress-induced vascular injury. Am J Respir Crit Care Med 2011;184:1030–40.
93. Citalan-Madrid AF, Vargas-Robles H, Garcia-Ponce A, et al. Cortactin deficiency causes increased RhoA/ROCK1-dependent actomyosin contractility, intestinal epithelial barrier dysfunction, and disproportionately severe DSS-induced colitis. Mucosal Immunol 2017;10:1237–47.
94. Plataki M, Hubmayr RD. The physical basis of ventilator-induced lung injury. Expert Rev Respir Med 2010;4:373–85.